



Prion-like C-Terminal Domain of TDP-43 and α -Synuclein Interact Synergistically to Generate Neurotoxic Hybrid Fibrils

Shailendra Dhakal¹, Courtney E. Wyant¹, Hannah E. George², Sarah E. Morgan² and Vijayaraghavan Rangachari^{1,3*}

1 - Department of Chemistry and Biochemistry, School of Mathematics and Natural Sciences, University of Southern Mississippi, Hattiesburg, MS 39406, USA

2 - School of Polymer Science and Engineering, University of Southern Mississippi, Hattiesburg, MS 39406, USA

3 - Center for Molecular and Cellular Biosciences, University of Southern Mississippi, Hattiesburg, MS 39406, USA

Correspondence to Vijayaraghavan Rangachari: Department of Chemistry and Biochemistry, School of Mathematics and Natural Sciences, University of Southern Mississippi, Hattiesburg, MS 39406, USA. vijay.rangachari@usm.edu (V. Rangachari)

<https://doi.org/10.1016/j.jmb.2021.166953>

Edited by Louise C. Serpell

Abstract

Aberrant aggregation and amyloid formation of tar DNA binding protein (TDP-43) and α -synuclein (α S) underlie frontotemporal dementia (FTD) and Parkinson's disease (PD), respectively. Amyloid inclusions of TDP-43 and α S are also commonly co-observed in amyotrophic lateral sclerosis (ALS), dementia with Lewy bodies (DLB) and Alzheimer disease (AD). Emerging evidence from cellular and animal models show colocalization of the TDP-43 and α S aggregates, raising the possibility of direct interactions and co-aggregation between the two proteins. In this report, we set out to answer this question by investigating the interactions between α S and prion-like pathogenic C-terminal domain of TDP-43 (TDP-43 PrLD). PrLD is an aggregation-prone fragment generated both by alternative splicing as well as aberrant proteolytic cleavage of full length TDP-43. Our results indicate that two proteins interact in a synergistic manner to augment each other's aggregation towards hybrid fibrils. While monomers, oligomers and sonicated fibrils of α S seed TDP-43 PrLD monomers, TDP-43 PrLD fibrils failed to seed α S monomers indicating selectivity in interactions. Furthermore, α S modulates liquid droplets formed by TDP-43 PrLD and RNA to promote insoluble amyloid aggregates. Importantly, the cross-seeded hybrid aggregates show greater cytotoxicity as compared to the individual homotypic aggregates suggesting that the interactions between the two proteins have a discernable impact on cellular functions. Together, these results bring forth insights into TDP-43 PrLD – α S interactions that could help explain clinical and pathological presentations in patients with co-morbidities involving the two proteins.

Published by Elsevier Ltd.

Introduction

Protein misfolding and toxic amyloid formation have come to define the pathogenesis of many neurodegenerative disorders including Alzheimer disease (AD), Parkinson's disease (PD), amyotrophic lateral sclerosis (ALS) and

frontotemporal dementia (FTD).^{1,2} Each of these pathologies is known to involve aberrant aggregation of a protein that brings to bear cellular abnormalities and toxicities. However, overlapping clinical presentations and comorbidities observed among patients with neurodegenerative diseases have motivated researchers into investigating the

possibility of molecular overlaps among the respective amyloidogenic proteins involved. For example, a wealth of evidence accrued over the years indicate that some of these maladies are accompanied by the deposition of common amyloid proteins such as tau and α -synuclein (α S), collectively referred to as tauopathies and synucleinopathies, respectively.^{3–5} Abnormal tau inclusions are often observed alongside amyloid- β (A β) deposits in AD patients⁶ as well as in conditions such as PD^{7,8} and prion disease.^{9,10} Similarly α S, the major protein involved in the formation of pathogenic amyloid inclusions of Lewy bodies (LBs) in PD is also observed in AD,¹¹ dementia with Lewy bodies (DLB), and multiple system atrophy (MSA).^{12,13} Like tau and α S, insoluble cytoplasmic inclusions of the ribonucleoprotein, tar DNA binding protein (TDP-43) are increasingly observed in many neurodegenerative pathologies such as ALS and FTD,¹⁴ as well as in patients with PD, DLB, and AD^{15,16}. There has been a surge in the reports on cross-interactions between amyloidogenic proteins such as the interactions between A β /tau, α S/A β , α S/tau,^{8,17–19} and prion/A β ,²⁰ which have cemented the hypothesis that cross-interaction mechanisms better define the underlying cause of neurodegenerative diseases and related co-pathogenesis. Along the same lines, recently it has come to light that α S and TDP-43 inclusions also co-exist in ALS, FTD and PD.^{15,21} While both α S and TDP-43 are known to independently form cytoplasmic amyloid inclusions,^{22–25} their co-existence raises the question of whether they interact with one another and if so, what consequence does such an interaction bring to bear. Indeed, recent reports do support this contention; TDP-43 was observed to synergistically interact and enhance α S toxicity in dopaminergic neurons,²⁶ while immunocytochemical and immunoblot analyses on mice models and SH-SY5Y neuroblastoma cells revealed that exogenous α S fibrils promote phosphorylation and aggregation of TDP-43.¹⁹ Furthermore, co-expression of TDP-43 and α S was shown to induce α S pathology in *C. elegans* that led to significant neurodegeneration as compared to their individual expressions.²⁷

α S is a 140 amino acid protein containing three regions; lipid binding N-terminal domain (NTD), an aggregation-prone non-amyloid component (NAC) middle region, and an intrinsically disordered, charged C-terminal domain (CTD). NAC and a part of NTD are the primary regions responsible for aggregation, while CTD seems to play an inhibitory role for this process.^{28,29} On the other hand, TDP-43 is a 414 amino acid containing ribonucleoprotein protein with an N-terminal domain, two RNA recognition motifs (RRMs), and a disordered prion-like C-terminal domain (PrLD) containing low complexity sequences.³⁰ TDP-43 is known to be involved in transcriptional regulation and RNA splicing.^{31,32} In pathology, the protein is translocated into the cytoplasm where it undergoes

aberrant proteolytic cleavage that generates different C-terminal fragments (CTFs; C35, C25, and C18), which consequently form toxic insoluble inclusions.^{33–38} Furthermore, under stress conditions, cytoplasmic TDP-43 undergoes liquid–liquid phase separation (LLPS) by coacervating with RNA and other proteins to form membraneless stress granules (SGs).^{39,40} If and how SGs play a role in the formation of cytoplasmic TDP-43 inclusions and cellular toxicity remains unclear. PrLD, a segment of such pathological aggregates, is primarily known to drive the fibrillization process and mediates protein–protein interactions.^{41,42} Despite multiple factors in regulating fibrillization of TDP-43 PrLD, a common biophysical phenomenon, liquid–liquid phase separation (LLPS) is also recently known to modulate the aggregation process via electrostatic interactions.⁴⁰

Here, we sought to determine how α S and TDP-43 interact with one another to exacerbate cellular toxicity, by investigating the full-length α S and TDP-43 PrLD as PrLD forms a key part of pathogenic proteolytic products of TDP-43 (Figure 1(a) and (b)). Our results indicate that α S and TDP-43 PrLD monomers, oligomers or fibrils cross-interact and modulate each other's aggregation behavior. Moreover, α S also enhance TDP-43 PrLD aggregation by modulating the liquid droplets formed by the phase separation of TDP-43 PrLD in presence of RNA. In all, cross-seeded aggregates show higher cytotoxicity than the individual aggregates suggesting the potential for such mechanisms to present greater pathogenicity.

Results

α S and TDP-43 PrLD monomers synergistically promote fibrillization

First, we questioned whether monomers of α S and TDP-43 PrLD are able to interact with one another. To answer this, heteronuclear multiple quantum coherence (HMQC) spectroscopy was performed on a uniformly ¹⁵N labeled α S and TDP-43 PrLD individually. Both proteins showed narrow chemical shift dispersions in the amide region (7.8–8.7 ppm for α S and 7.7–8.5 for TDP-43 PrLD in the ¹H dimension) confirming the well-known disordered structures for both the proteins (blue; Figure 1(c) and (d)). To see whether the two proteins interact with one another, HMQC spectra of the ¹⁵N-enriched proteins were observed upon incubating with unlabeled, natural isotope-abundant proteins in equimolar concentrations at 37 °C. The spectrum of α S co-incubated with unlabeled TDP-43 PrLD showed disappearance of several cross-peaks along with significant changes in the chemical shifts (Figure 1(c)). The disappearance of peaks is largely attributed to the aggregation of proteins which often leads to significant line broadening and/or loss of signal intensities.^{43,44} Interestingly, large

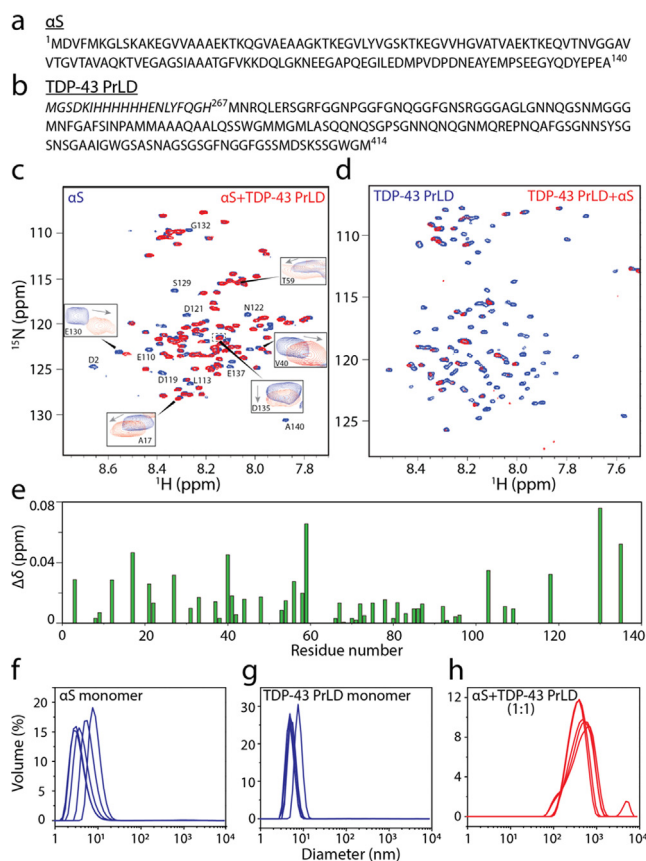


Figure 1. ^1H - ^{15}N HMQC spectroscopy of αS and TDP-43 PrLD along with DLS of respective reactions. a-b) Sequence of full-length 1–140 amino acid residues αS (a) and 267–414 amino acid residues TDP-43 PrLD used in the experiment. c) ^1H - ^{15}N HMQC of $10\ \mu\text{M}$ ^{15}N -labeled αS monomers alone (blue) or in the presence of unlabeled $10\ \mu\text{M}$ TDP-43 PrLD monomers (red) in $20\ \text{mM}$ MES buffer pH 6.0 at $37\ ^\circ\text{C}$. Some of the residues undergoing chemical shift perturbations (CSPs) are shown in boxes while those with lost peaks are indicated by letters without boxes. d) ^1H - ^{15}N HMQC of $10\ \mu\text{M}$ ^{15}N -labeled TDP-43 PrLD monomers alone (blue) or in presence of unlabeled αS (red). e) CSPs for equimolar incubations of αS and TDP-43 PrLD that were calculated using the equation, $\Delta\delta = \sqrt{(\delta H)^2 + 0.14(\delta N)^2}$ from the spectrum in (c). f-g) DLS histograms of $10\ \mu\text{M}$ αS monomer control, TDP-43 PrLD monomer control and co-incubated mixture 1:1 αS and TDP-43 PrLD in the same buffer and temperature conditions taken within 10 min of incubation.

shifts in cross-peaks appear to be more on the N- and C-terminal domains of αS (residues 1–60 and 100–140; boxes, Figure 1(c)). Considering that the N- and C-terminal domains are charged and NAC domain of αS is prone to amyloid formation, it is possible that TDP-43 PrLD induces aggregation of the NAC domain αS . Similarly, a substantial signal loss of cross-peaks was observed for TDP-43 PrLD upon co-incubation with αS indicating potential aggregation of the former (Figure 1(d)). In order to confirm the NMR observations, aggregation of the co-incubated samples was analyzed by dynamic light scattering (DLS) analysis. The freshly fractionated control monomers of αS and TDP-43 PrLD showed a hydrodynamic diameter of $\sim 5\ \text{nm}$ individually (Figure 1(f) and (g)). One has to bear in mind that even the SEC fractionated monomers may be a mixture containing a small percentage of small oligomers. In contrast, the co-incubated samples

showed aggregation with an average diameter of $>10^3\ \text{nm}$ within 10 min of incubation (Figure 1(h)). These results confirm the NMR observations that αS and TDP-43 PrLD interact with one another to promote high molecular weight aggregates. Encouraged by these NMR results, a deeper investigation into the dynamics of interactions between the two proteins by means of T_2 relaxations and H/D exchange will be carried out and will be reported in the near future, but the data obtained so far unequivocally indicates the interactions between αS and TDP-43 PrLD.

To further understand the mechanism of αS and TDP-43 PrLD interactions, we set forth to investigate the aggregation kinetics using thioflavin T (ThT) fluorescence assay (Figure 2). In one reaction set, αS concentration was held constant at $20\ \mu\text{M}$ while TDP-43 PrLD concentrations were increased from 1 to $20\ \mu\text{M}$

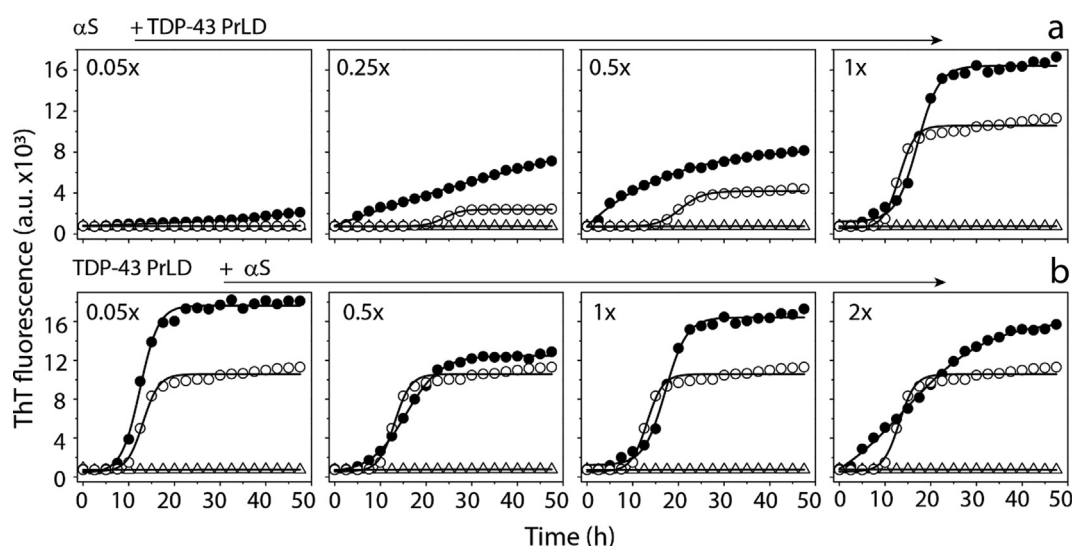


Figure 2. ThT aggregation kinetics of monomeric α S and TDP-43 PrLD in 20 mM MES buffer at pH 6.0 a) ThT fluorescence of 20 μ M α S (Δ) in presence of 0.05 to 1 molar ratio of TDP-43 PrLD to α S (\bullet) and respective TDP-43 PrLD controls (\circ). b) ThT fluorescence of 20 μ M TDP-43 PrLD (\circ) in presence of 0.05 to 2 molar ratio of α S to TDP-43 PrLD (\bullet) and respective α S controls (Δ). The data were fit with Boltzmann's sigmoidal function (see Materials and Methods) to derive lag time information.

(0.05, 0.25, 0.5 and 1.0 molar equivalents). The reactions were incubated at 37 $^{\circ}$ C and the kinetics of aggregation was monitored for 48 h (Figure 2 (a)). All the data points were plotted and fitted using the Boltzmann sigmoidal fit (see Methods). The control α S did not show any aggregation during this period (Δ ; Figure 2(a)). Similarly, at the lowest concentration (1 μ M), TDP-43 PrLD control did not show increase in ThT fluorescence (Figure 2(a)). TDP-43 PrLD control at 5, 10, and 20 μ M showed concentration-dependent aggregation with aggregation lag times of 20, 15.4, and 9.6 h, respectively; (\circ ; Figure 2(a)), while the co-incubated samples with α S showed significantly decreased lag times (\bullet ; Figure 2(a)) suggesting synergistic augmentation of aggregation between the two proteins. In addition, the co-incubated samples showed higher ThT intensities, which could either indicate numerically more fibrils or an increased ThT binding vis-à-vis higher fluorescence per fibrils formed by both α S and TDP-43 PrLD. Next, to investigate whether α S can modulate the aggregation behavior of TDP-43 PrLD, TDP-43 PrLD was held constant at 20 μ M and α S concentrations were increased from 1 to 40 μ M (0.05, 0.5, 1 or 2 molar equivalents) (Figure 2(b)). TDP-43 PrLD control aggregated with lag time of 9.6 h (\circ ; Figure 2(b)) while α S did not show aggregation within the 50-h window (Δ ; Figure 2(b)). There were small but discernable decreases in TDP-43 PrLD lag time of aggregation with the proportional increase in ThT fluorescence intensities with increasing α S (\bullet ; Figure 2(b)). This effect was most prominent with the 40 μ M α S incubation, which led to no

detectable lag time in TDP-43 PrLD (\bullet ; Figure 2 (b)).

In order to monitor the effect of sub-stoichiometric co-incubations of the two proteins, higher concentration of α S at 50 μ M was incubated in presence of 5 μ M (0.1x molar equivalents) and 2 μ M (0.04x molar equivalents) TDP-43 PrLD. The reverse incubations with a higher concentration of TDP-43 PrLD were prohibitively difficult due to the increased aggregation propensity of the protein that showed lag time of smaller than three hours for 50 μ M TDP-43 PrLD (data not shown). The reactions containing co-incubations of 50 μ M α S with sub-stoichiometric TDP-43 PrLD showed significant decreases in lag time of α S fibrillization as compared to either α S or TDP-43 PrLD controls (Figure 3(a)). The co-incubation with 0.1 and 0.04 molar equivalents showed lag times of 10 and 20 h, respectively (Figure 3(a)) suggesting TDP-43 PrLD promotes significant aggregation of α S. After 72 h of incubation, reaction samples were centrifuged at 18,000g for 20 min to sediment fibrils formed, if any. Both the samples before centrifugation and supernatant of centrifuged samples were then subjected to immunoblot analysis using Syn211 monoclonal α S antibody (Figure 3(b)). The blot showed the presence of a band corresponding to >260 kDa that failed to enter the gel in both co-incubated samples (T; Figure 3(b)) in addition to monomeric, dimeric, and trimeric α S present in all the samples. The corresponding supernatant samples did not contain this high molecular weight band (S; Figure 3(b)) confirming that the high molecular weight species are sedimentable aggregates or

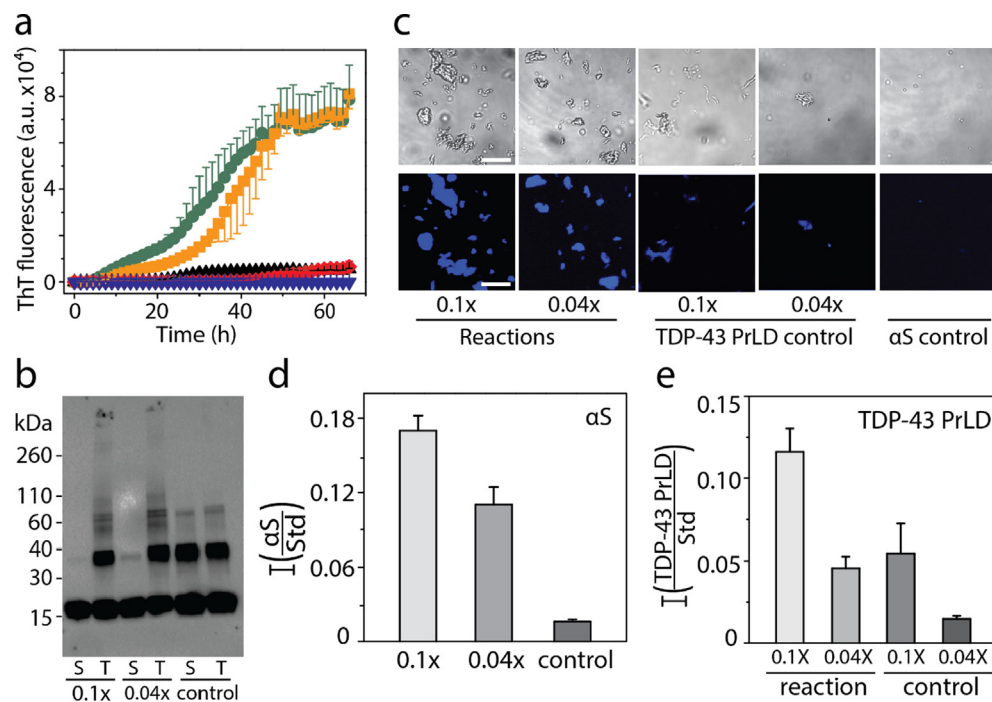


Figure 3. Interaction of monomeric TDP-43 PrLD and α S in 20 mM MES buffer pH 6.0. (a) ThT fluorescence kinetics of 50 μ M α S alone (\blacktriangledown) and in presence of 0.04 (\blacksquare) and 0.1 (\bullet) molar ratio of TDP-43 PrLD to α S, and respective 0.04 (\blacklozenge) and 0.1 (\blacktriangle) TDP-43 PrLD controls. (b) Western blot of ThT reactions using α S antibodies. Aliquot of sample from the reaction at 72 h was subjected to western blot as total sample (T), and supernatant (S) after centrifuging at 18,000g (c) Representative fluorescence microscopic images of Thioflavin S (ThS) stained α S and TDP-43 PrLD aggregation reactions at 72 h after centrifuging at 18,000g (Scale bar = 20 μ m). (d and e) Relative quantification of α S and TDP-43 PrLD to the Cytochrome C internal standard in pellet of reactions and control at 72 h after centrifugation at 18,000g; 0.1x and 0.04x indicates molar ratio of TDP-43 PrLD to α S.

fibrils. To further ascertain the presence of α S fibrils in the co-incubated samples, differential interference contrast (DIC) microscopy analysis of the fibrils was employed. The pellet obtained from the samples centrifuged after 72 h was resuspended in 20 mM MES buffer pH 6.0 and incubated with 10 μ M thioflavin-S (ThS) and imaged after 10 min. The images revealed the presence of higher ThS positive fibrils in the reaction compared to TDP-43 PrLD and α S controls (Figure 3(c)). Further quantitative analysis was carried out to quantitatively assess the proteins present in the fibrils using MALDI-ToF. Relative quantitation was performed using a known amount of cytochrome C (1.42 μ mol) as an external standard that was co-analyzed with the samples in the mass spectrometer (Figure S1). Analysis of the data obtained revealed that the relative amounts of α S in the pellet of reactions containing 0.1 and 0.04 molar equivalents of TDP-43 PrLD were higher compared to the individual protein controls (Figure 3(d)). However, α S amount in the supernatant of the control reaction was significantly higher compared to the reactions in α S fibrillization upon co-incubation with TDP-43 PrLD. Similar relative quantification of TDP-43

PrLD to standard in the pellets of reaction showed a higher amount of TDP-43 PrLD than the respective controls indicating enhanced fibrillization in presence of α S (Figure 3(e)). Since, both α S and TDP-43 PrLD were co-observed within the sedimentable pellets of the cross-seeding reactions, we performed qualitative and quantitative analyses to investigate the presence of hybrid aggregates. For qualitative analysis, 20 μ M TDP-43 PrLD was incubated with 2 μ M α S at 37 $^{\circ}$ C for 20 h and probed using dot blot analysis using both α S and TDP-43 antibodies. We reasoned that since α S does not aggregate within 72 h (Figure 3(a)); especially at low concentrations, co-incubation with TDP-43 PrLD will eliminate the possibility of homotypic α S fibrils in 20 h. Any α S fibrils thus observed will have to be due to co-aggregation with TDP-43 PrLD. As expected, the dot blot analysis of the sample using α S and TDP-43 antibodies showed presence of both α S and TDP-43 PrLD confirming that α S co-aggregates with TDP-43 PrLD during fibrils formation (Figure S2(a)). Then quantitative analysis of the aggregates was done by examining the stoichiometric ratios of two proteins in the pellets of co-incubated sample containing equimolar (20 μ M) α S and TDP-43 PrLD at 37 $^{\circ}$ C.

The volume of the reaction was kept high (500 μL) to recover sufficient amount of fibrils. Fibrils were then isolated by centrifuging the sample after 7.5 h, the time where the co-incubated reaction had aggregated faster than the individual proteins (Figure S2(b) inset). Quantitative MALDI-ToF analysis using cytochrome C as standard revealed the presence of both proteins in the fibrils at 1:1.2 ratio of αS to TDP-43 PrLD (Figure S2(b)). This equimolar distribution of the proteins in the sedimented pellet is unequivocally indicative of the formation of hybrid αS -TDP-43 fibrils. Taken together, the data indicate that both αS and TDP-43 PrLD monomers interact with one another and promote fibrillization synergistically.

αS oligomers and sonicated fibrils seed fibrillation of TDP-43 PrLD monomers but αS monomers are innocuous to seeding by TDP-43 PrLD sonicated fibrils

Having established that monomers of αS and TDP-43 PrLD interact and promote each other's aggregation, we questioned if their interactions are restricted to only monomers or whether oligomers and sonicated fibrils can also cross-seed respective monomers. To answer these questions, dihydroxyphenyl acetaldehyde (DOPAL), a metabolite of dopamine biogenesis, induced oligomers of αS were used as *de facto* oligomers along with sonicated fibrils of both αS and TDP-43 PrLD. Isolation of stable oligomers of TDP-43 PrLD was not successful and hence were excluded from the investigation. DOPAL-derived oligomers of αS were generated and isolated by size exclusion chromatography (see Materials and Methods). The αS oligomers showed a monodisperse peak in dynamic light scattering (DLS) around 10 nm diameter (Figure 4(a)) with a molecular weight centered at ~ 48 kDa (~ 3 mer) observed in immunoblot along with two faint bands corresponding to ~ 33 and 64 kDa species (2 and 4mers, respectively) (inset; Figure 4(a)). Moreover, circular dichroism (CD) spectra of the αS oligomers showed random coiled structure with characteristic minima at 195 nm (Figure 4(b)) while morphologically they are seen as punctate spheres of ~ 4 –6 nm height by atomic force microscopy (AFM) (inset; Figure 4(b)). Incubation of these oligomers at 0.5 and 1 μM concentrations with 15 μM of monomeric TDP-43 PrLD in 20 mM MES at pH 6.0 resulted in decrease in lag time of TDP-43 PrLD aggregation to ~ 6 h (Figure 4(c)). Immunoblot analysis of the samples after 12 h showed the formation of high molecular weight fibril bands that is absent in the control sample of TDP-43 PrLD (inset; Figure 4(c)), clearly indicating that αS oligomers are able to seed TDP-43 PrLD monomers. Seeding of 20 μM monomers of either αS or TDP-43 PrLD with 1, 2 or 4 μM sonicated fibrils of TDP-43 PrLD or αS , respectively showed different behavior. Homotypic

seeding of αS monomers by αS sonicated fibrils showed an immediate increase in ThT intensities as expected for seeding by elongation mechanism⁴⁵ (Figure 4(d)). In contrast, the seeding of TDP-43 PrLD monomers by αS sonicated fibrils displayed a more sigmoidal response (Figure 4(d)) but with a shorter lag time of ThT fluorescence to that of the TDP-43 PrLD control. This suggests that TDP-43 PrLD monomers may undergo conformational alterations before they grow on αS fibrils. Similarly, homotypic seeding of TDP-43 PrLD monomers by TDP-43 sonicated fibrils showed immediate and substantial increases in ThT intensities (Figure 4(e)). But in stark contrast, seeding of αS monomers by TDP-43 PrLD sonicated fibrils failed to show interactions (Figure 4(e)). The secondary structure of the cross-seeded reactions from (c-e) was analyzed by FTIR (Figure 4(f)). The cross-seeded reaction of TDP-43 PrLD monomers with αS sonicated fibrils or DOPAL-derived αS oligomers displayed a β -sheet structure with an absorbance peak centered at 1615 cm^{-1} (pink and black; Figure 4(f)) as opposed to the monomeric samples that show predominantly random coil structure at 1643 cm^{-1} or 1650 cm^{-1} (blue and red; Figure 4(f)). In contrast, seeding of αS monomers with TDP-43 PrLD fibrils showed a predominant random coil structure at 1643 cm^{-1} (green; Figure 4(f)) suggesting minimal or no seeding. Finally, morphological features of the seeded aggregates were investigated by AFM. Sonicated fibrils of αS and TDP-43 PrLD showed fragmented aggregates as expected (Figure 4(g) and (i)). TDP-43 PrLD monomers seeded with sonicated αS fibrils after 8 h of incubation showed smooth fibrils (Figure 4(h)). However, αS monomers seeded with TDP-43 PrLD fibrils did not show fibers after 8 h of incubation (Figure 4(j)). These results are in agreement with kinetics data supporting the observation of the difference in the ability to seed. Together, these data suggest that while TDP-43 PrLD monomers seem to be amenable for seeding by different αS species, αS monomers are selective towards TDP-43 PrLD monomers and not sonicated fibrils.

αS modulates LLPS of TDP-43 PrLD and RNA and induces insoluble aggregates

One of the pivotal roles of TDP-43 in pathophysiology is that under cellular stress conditions, they are known to coacervate with RNA and other proteins to undergo LLPS to form stress granules (SGs) in the cytoplasm.^{39,46} To see whether αS is able to modulate LLPS, TDP-43 PrLD was labeled with Hilyte-647 and mixed with unlabeled TDP-43 PrLD at 1% molar ratio (0.2 μM) to a final total concentration of 20 μM protein. Similarly, αS was labeled with Hilyte-405 and mixed with unlabeled protein in 1:99 ratio, and this sample was used at final concentrations of 5 and 1 μM in 20 mM MES buffer at pH 6.0 at 37 $^{\circ}\text{C}$. As expected, TDP-43 PrLD spontaneously phase separates in pres-

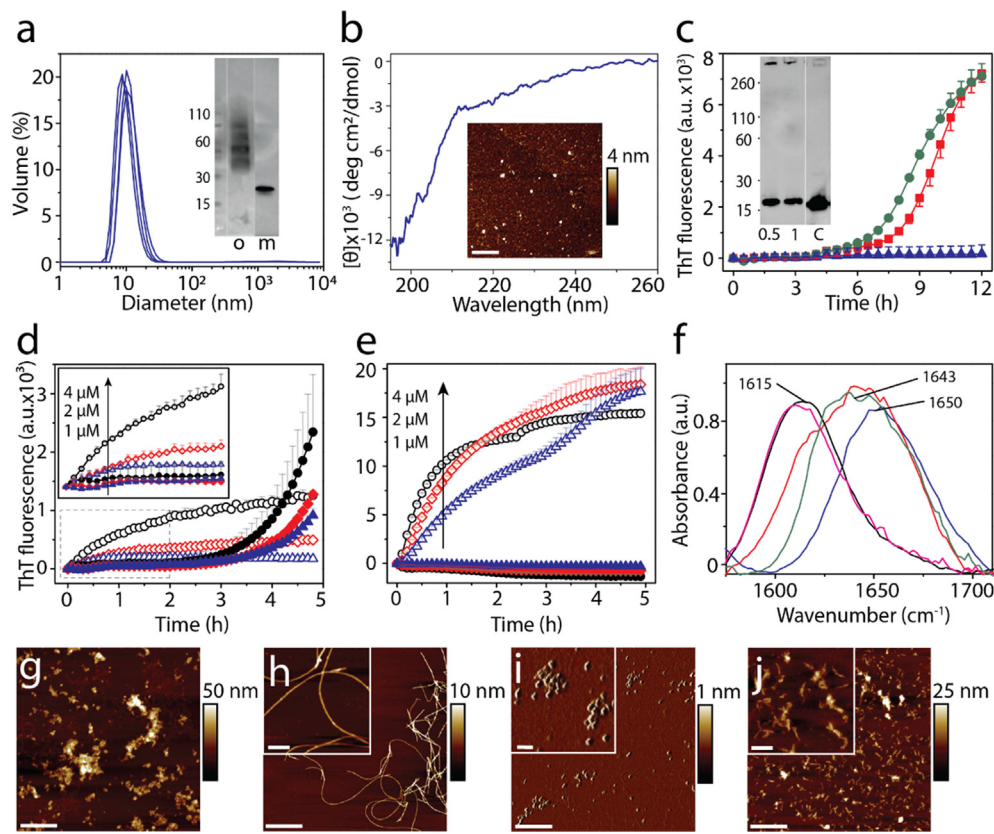


Figure 4. Cross-seeding of oligomers and sonicated fibrils with monomers. a) DLS analysis of DOPAL-derived α S oligomers isolated from SEC. (inset) SEC fraction containing the oligomer ‘o’ used in the study; ‘m’ refers to control monomer. b) CD spectra and AFM height image (inset) of DOPAL-derived α S oligomers used for cross-seeding reaction (scale bar = 1 μ m). Cross-seeding reactions with monomers of 15 μ M TDP-43 PrLD alone (\blacktriangle) or in the presence of 0.5 μ M (\blacksquare) or 1 μ M (\bullet) DOPAL-derived α S oligomers in the presence of 10 μ M ThT. (inset) immunoblot of the reaction after 12 h probed with TDP-43 antibody; ‘c’ refers to TDP-43 PrLD monomer control. d) Seeding of 20 μ M α S monomers with 4 μ M (\bullet), 2 μ M (\diamond), and 1 μ M (\triangle) of α S sonicated fibrils, and 20 μ M TDP-43 PrLD monomers seeded with 4 μ M (\bullet), 2 μ M (\diamond), and 1 μ M (\triangle) of α S sonicated fibrils. e) Seeding of 20 μ M TDP-43 PrLD monomers with 4 μ M (\bullet), 2 μ M (\diamond), and 1 μ M (\triangle) of TDP-43 PrLD sonicated fibrils and seeding of 20 μ M α S monomers with 4 μ M (\bullet), 2 μ M (\diamond), 1 μ M (\triangle) of TDP-43 PrLD seed. f) FTIR analysis of cross-seeding reactions from (c-e). TDP-43 PrLD monomers cross-seeded with 1 μ M DOPAL-derived α S oligomers after 12 h of incubation (—); TDP-43 PrLD monomers seeded with 1 μ M α S sonicated fibrils (—); α S monomers seeded with 1 μ M TDP-43 PrLD sonicated fibrils (—) along with controls such as α S monomers (—) and TDP-43 PrLD monomers (—) (g-j) AFM height image of α S sonicated fibrils (g), α S sonicated fibrils seeded TDP-43 PrLD monomers (h), TDP-43 PrLD sonicated fibrils (i), and TDP-43 PrLD sonicated fibrils seeded α S monomers (j) (scale bar = 1 μ m, inset = 200 nm).

ence of RNA to form liquid droplets (0 h; **Figure 5** (a)). The addition of α S led to instant changes in the morphology of the droplets to become somewhat distorted, non-spherical structures in both stoichiometric incubations (0 h; **Figure 5**(a)). The same reactions monitored after 24 h showed the droplets becoming more distorted and aggregated as opposed to the control, which continued to have well-defined phase-separated liquid droplets (24 h; **Figure 5**(a)). To investigate whether the droplet deformity is due to aggregation, the dynamics of liquid droplets were probed by fluorescence recovery after photobleaching (FRAP) analysis. The control TDP-43 PrLD – RNA droplets showed significant FRAP recovery rates both at 0 h and 24 h indicating

that the samples retained significant fluid characteristics (**Figure 5**(b) and (c)). However, the FRAP recovery rates of α S co-incubated TDP-43 PrLD droplets reduced significantly at 0 h which remained constant over the period of 24 h with a more dramatic effect with 5 μ M than 1 μ M α S (**Figure 5**(b) and (c)), which suggest gelation or aggregation samples. To unambiguously confirm if the attenuation of droplet fluidity is due to aggregation, the same reactions were monitored by ThT. The data indicated that the ThT fluorescence did not show much increase in 24 h for the TDP-43 PrLD–RNA control reaction (\circ ; **Figure 5**(d)). In contrast, samples co-incubated with α S showed increased ThT fluorescence suggesting aggregation of TDP-43

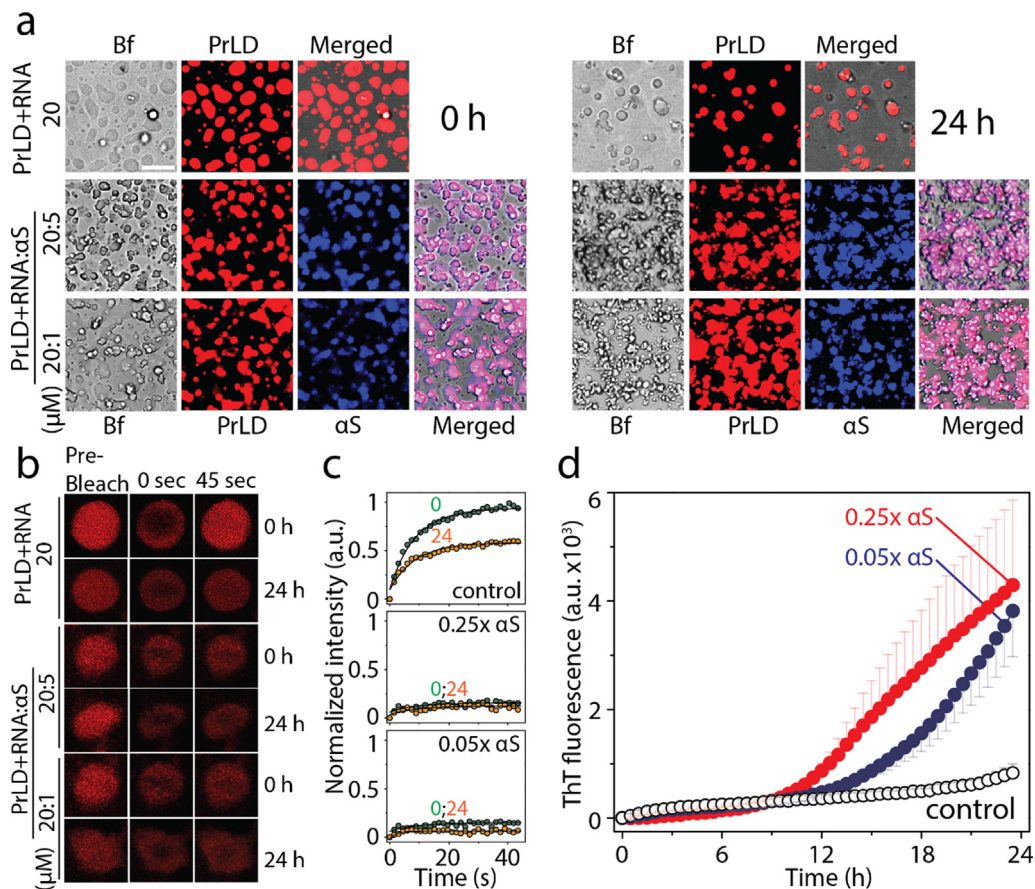


Figure 5. Modulation of TDP-43 PrLD LLPS by α S. (a) Timestamped confocal images of the co-incubations of Hilyte-647 labelled TDP-43 PrLD (20 μ M) and RNA (40 μ g/mL) in the absence and presence of Hilyte 405 labelled α S (5 or 1 μ M) in 20 mM MES buffer pH 6.0 at 37 $^{\circ}$ C; Bf represents 'bright field'. (b) FRAP analysis on the selected droplets from the reactions before (pre-bleach), during (0 sec), and after photobleaching (45 sec), immediately after incubation (0 h) and after 24 h. (c) Normalized kinetics of fluorescence recovery data obtained from FRAP intensity; TDP-43 PrLD and RNA control reaction along with 5 μ M and 1 μ M α S at 0 h (●) and after 24 h (○). The data was fit to a first order exponential growth equation (solid lines). (d) Corresponding ThT fluorescence kinetics of the reactions; TDP-43 PrLD and RNA (○) control reaction along with sub-stoichiometric, 1 μ M (●) or 5 μ M (●) α S incubations.

PrLD as observed in other reactions (● and ●; Figure 5(d)). Taken together, these data suggest that α S modulate phase separation of TDP-43 PrLD with RNA and enhance its aggregation.

Cross-seeded heterotypic fibrils are more cytotoxic than the homotypic fibrils of α S or TDP-43 PrLD.

Recently, it was found that TDP-43 enhances the toxicity of α S in dopaminergic neurons resulting in neurodegeneration.²⁶ Thus, we wanted to investigate and compare the toxicities of heterotypic fibrils formed by cross-seeding and the homotypic ones formed by individual α S or TDP-43 PrLD fibrils in human neuroblastoma SH-SY5Y cells. In order to accomplish this, 20 μ M α S monomers were co-incubated with 5 μ M TDP-43 PrLD monomers (TDP-43 PrLD: α S = 1:4) in quiescent conditions for 24 h at 37 $^{\circ}$ C. Similarly, 20 μ M TDP-43 PrLD

monomers were co-incubated with 5 μ M α S monomers (TDP-43 PrLD: α S = 4:1) under identical conditions. The samples were then diluted five-folds and incubated with freshly cultured SH-SY5Y cells for additional 24 h. Appropriate control reactions corresponding to homotypic proteins were also set up and incubated under similar conditions. Cell viability of the confluent cells was then determined by XTT assay (see Materials and Methods).⁴⁷ The results indicate that in both stoichiometries, only the co-incubated samples showed higher toxicity than the homotypic aggregates (Figure 6). Among the two, 1:4 reaction of TDP-43 PrLD: α S monomers showed a substantially greater degree of toxicity (~40%) as compared to the 4:1 sample (~28%), suggesting that the effect of sub-stoichiometric addition of TDP-43 PrLD enhances α S aggregation and toxicity. In case of cross-seeding of fibrils to monomers, α S fibrils seeded TDP-43 PrLD aggregation showed a substantial increase in toxicity

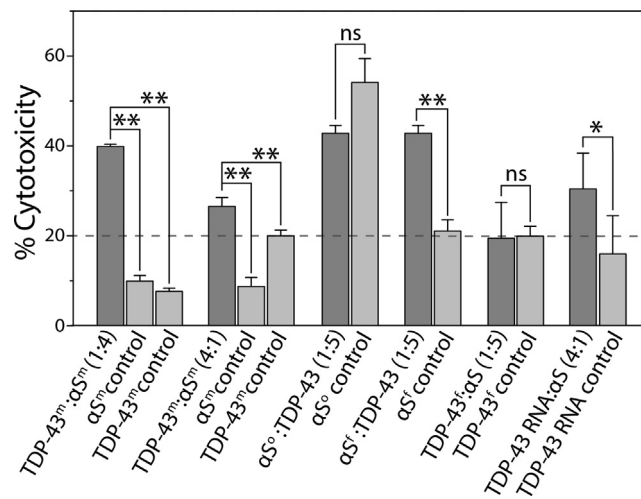


Figure 6. Cytotoxicity of monomeric α S and TDP-43 PrLD species along with homotypic and heterotypic fibrillar species of α S and TDP-43 in SH-SY5Y cells by XTT assay. 'm', 'o' and 'f' in the superscript represents monomer, oligomer, and sonicated fibril respectively. All the data were obtained in triplicates, * represents $p < 0.1$ and ** represents $p < 0.01$ based on one-way ANOVA analysis.

(~41%) compared to the α S fibril seeds or TDP-43 PrLD monomers (<20%) (Figure 6). TDP-43 PrLD fibril seeded α S aggregation did not show an increase in toxicity compared to the controls. These results correlate with the kinetics and morphology of the seeding reaction in which only α S fibrils seeded TDP-43 PrLD aggregation showed aggregation (Figure 4). Similarly, the addition of α S monomers to the liquid droplets of TDP-43 PrLD and RNA that promoted insoluble fibrils also showed an increase in toxicity (~30%) as compared to TDP-43 PrLD-RNA control (<20%). In contrast to these results, only α S oligomer (DOPAL-induced) seeded TDP-43 PrLD fibrils did not show a statistically significant increase in toxicity (Figure 6). One of the main reasons for this result is due to the fact that α S oligomer is DOPAL-induced and not a bonafide aggregation pathway intermediate; clearly, DOPAL-induced α S oligomers showed maximum toxicity (~57%; Figure 6). Therefore, it is possible that fibrils of TDP-43 PrLD seeded by these oligomers do not display any higher degree of toxicity. Together, these data suggest that the synergistic interactions between TDP-43 PrLD and α S lead to the formation of hybrid fibrils which are more toxic than those of their individual proteins.

Discussion

The work reported here is focused on the effects of TDP-43 PrLD on α S and vice versa. We chose to focus on PrLD instead of the full-length TDP-43 for a variety of reasons; First, the post-mortem ALS and FTD brain tissues show an abundance of TDP-43CTFs ranging between 35 and 18 kDa (35, 25, 20, and 18 kDa),^{48–51} all of which constitute PrLD (17 kDa) a major part. In a more recent study

on mass spectrometric analysis of post-mortem brain samples, enhanced levels TDP-43 C-terminal truncation fragment of 266–414 (corresponds to TDP-43 PrLD) was observed in ALS and AD patients.³⁸ Second, TDP-43 CTFs are primarily involved in the formation of cytoplasmic inclusions generated upon aberrant proteolytic cleavage of the full-length TDP-43 under pathological conditions in which PrLD plays a major role.^{33,42,52} Third, CTFs ranging between 35 and 18 kDa are also produced by alternative splicing of TDP-43 mRNA and are linked to pathology.^{51,53} Fourth, the PrLD of TDP-43 is known to play a major role in SG formation, aggregation as well as protein–protein interactions.^{54–56} Lastly, almost all pathogenic mutations lie within PrLD^{42,57} implying its significance in pathophysiology.

The results presented here demonstrate synergistic interactions between TDP-43 PrLD and α S, which in part, recapitulate the pathobiological observations. Rapid aggregation of the two protein monomers upon co-incubation (Figure 1(g)), and the concomitant increases in α S or TDP-43 PrLD aggregation rates (Figure 2) suggest a synergistic aggregation possibly during nucleation. In addition, seeding of TDP-43 PrLD by both oligomers and sonicated fibrils of α S also shows cross-interaction between the two proteins. These results collectively suggest a possible hetero-nucleation mechanism predominating at the initial stages of aggregation and elongation mechanism at the later stages. The results also bring out mechanistic differences in their interactions; the data indicate that the three key α S species such as monomers, oligomers and sonicated fibrils are indiscriminate in interacting with and getting modulated by TDP-43 PrLD monomers (Figure 7). However, only monomeric TDP-43 PrLD, and not

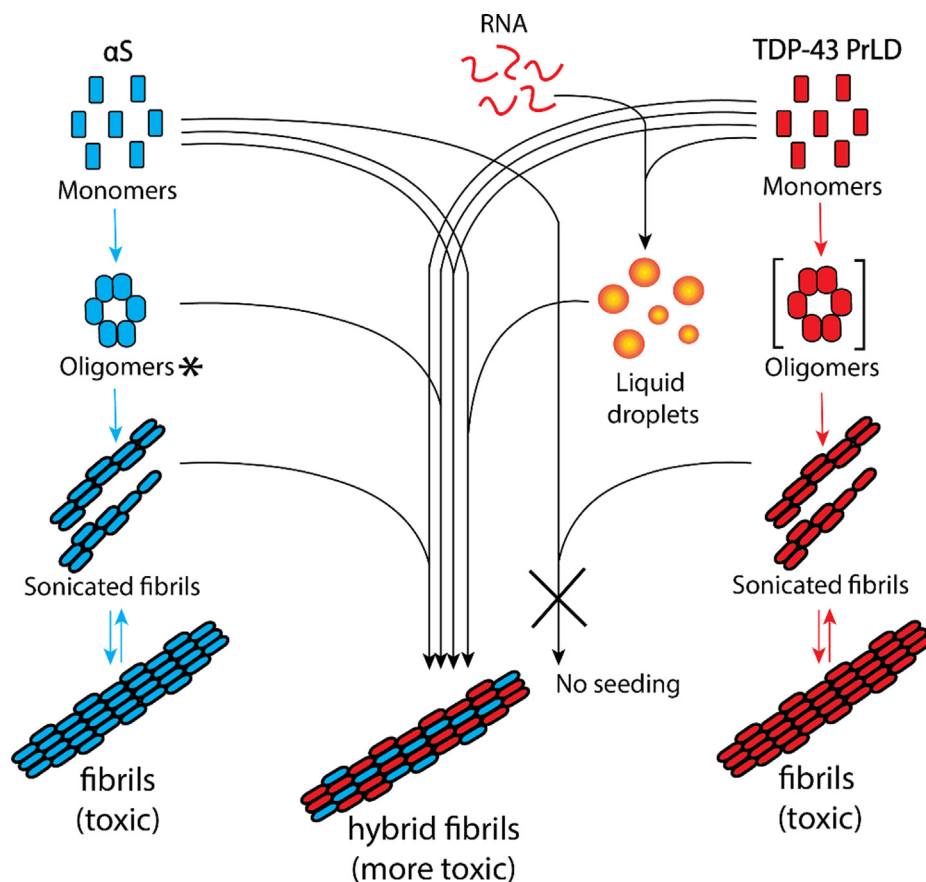


Figure 7. Schematic diagram summarizing the collective results from this work. The square parenthesis indicates theoretical transient oligomers and not used in this study. ****** DOPAL-derived *de facto* intermediate oligomers but shown along the aggregation pathway for simplicity.

the sonicated fibrils, seem to preferentially interact with α S monomers and aggregates (Figure 7). From these results, one may conjecture that early stages of TDP-43 proteinopathies may be susceptible to modulation by the presence of α S aggregates in the form of Lewy bodies. Furthermore, the interaction of TDP-43 PrLD and α S monomers seem to be cooperative with both assisting one another in promoting high molecular weight aggregates expeditiously. We also deduce that co-incubation of monomers is likely to form α S-TDP-43 PrLD hybrid aggregates based on both qualitative and quantitative evidence (Figure S2(a) and (b)); a) synergistic augmentation in the rate of aggregation of both proteins, and b) the observed molar equivalents of both proteins within the sediments fibrils. However, the data also show that α S monomer, oligomer and fibrils are equally capable of interacting with TDP-43 PrLD monomers (Figure 7) and hence, the possibility of mechanisms such as nucleation-assisted aggregation and protofibril elongations are likely between the two proteins as mentioned earlier. But one also cannot discount other possible

mechanisms such as heterologous secondary nucleation, fibril fragmentations and epitaxial growth, which remain to be investigated. Another interesting observation is that the effect of TDP-43 PrLD on α S is far more pronounced than vice versa. This is partly due to α S being relatively slow to aggregate as compared to TDP-43 PrLD; for example, the lag times for α S and TDP-PrLD (20 μ M) aggregation at 37 $^{\circ}$ C and in identical quiescent buffer conditions are >7 days and 8 h, respectively (data not shown). Therefore, augmentation of α S aggregation by TDP-43 PrLD is readily comprehensible as the lag time of aggregation is reduced to 20 h from weeks (Figure 3(a)). On the other hand, the effect of α S on TDP43 PrLD is discernable but subtle (Figure 2 (b)). This is especially true with DOPAL-derived α S aggregates which augment TDP-43 PrLD aggregation significantly (Figure 4(c)). Previous studies have shown that the interaction of dopamine with α S results in the formation of structurally distinct oligomers.^{58,59} In particular, small angle X-ray scattering of α S trimers formed in the presence of dopamine has revealed worm-like shape due to laterally associated monomers

without end-to-end arrangement.⁶⁰ Such trimers are different from those formed in the absence of dopamine exhibiting spherical, chain like or ring like annular structure. Along similar lines, we anticipate that DOPAL-derived α S oligomers will be different both structurally and functionally mainly based on the fact that DOPAL forms covalent, Schiff's base adduct with α S. α S sonicated fibrils seeding of TDP-43 PrLD monomers show a cooperative mechanism with a delay in elongation, which could indicate conformational reorganization of TDP-43 monomers induced by α S sonicated fibrils. On the other hand, TDP-43 PrLD sonicated fibrils failed to interact with α S monomers suggesting possible incompatibility of TDP-43 PrLD sonicated fibrils structure to seed. Clues about the structural basis of interactions come from the NMR data, which shows that the TDP-43 PrLD seem to preferentially interact with α S on the N-terminal and C-terminal ends of the protein (1–60 and 100–140, respectively) based on the large chemical shift changes observed, while augmenting aggregation via the amyloidogenic core NAC region (61–95) (Figure 1 (c)). This is readily comprehensible given that the N- and C-terminal ends of α S are hydrophilic and acidic, they could interact electrostatically with highly positively charged TDP-43 PrLD bringing the amyloidogenic NAC region of α S in close proximity to augment aggregation. Unfortunately, similar structural information on TDP-43 PrLD was undecipherable due to rapid aggregation of TDP-43 PrLD and consequent dilution of chemical shifts. Collectively, these data bring forth the synergistic yet selective interactions between broad categories of α S and TDP-43 PrLD species. Yet another significant aspect that highlights the interaction between the two proteins is the ability of α S to modulate LLPS of TDP-43 PrLD and RNA and promote insoluble aggregates. Since these droplets are the main constituents of cytoplasmic SGs, these results demonstrate crucial yet hitherto unseen interactions that may hold significance in neurodegenerative diseases with co-morbidities. Perhaps the most significant of all is the observation that only the hybrid aggregates show far greater cellular toxicity as opposed to the individual aggregates, which suggests that co-morbidities in these pathologies are better defined by the cross-talk between TDP-43 and α S.

It is well-known that aggregates of α S and TDP-43 individually are observed in many neurodegenerative pathologies including AD, PD, Huntington's disease, FTD, etc.^{11,61–63} The term 'synucleinopathies' has come to define some of the pathologies in which α S aggregates play a causative or a propagative role(s). In the last decade, aggregates of TDP-43 have also been increasingly observed in as many pathologies in which α S aggregates have been observed¹⁵ invoking a compelling argument to categorize some of these maladies as TDP-43 proteinopathies. However, more

interesting is the significant overlap between pathologies in which both aggregates of TDP-43 and α S aggregates are observed. Indeed, many reports have indicated the colocalization of TDP-43 and α S aggregates^{27,64} implicating potential interactions between the two proteins to play a role in these pathologies. The data presented here unequivocally demonstrate the interactions between these two proteins which may underlie the clinical and pathological observations, and open doors to deeper investigations in establishing mechanistic links to co-morbidities in neurodegenerative diseases.

Methods

Expression and purification of recombinant proteins

Expression and purification of both unlabeled and ¹⁵N labeled recombinant TDP-43 PrLD was performed as described previously.⁴⁰ TDP-43 PrLD fusion construct (Addgene plasmid #98669) with hexahistidine tag followed by tobacco etch virus (TEV) cleavage site at N-terminus was transformed in BL21 Star™ (DE3) cells, protein expression was induced using 0.5 mM IPTG (Life Technologies) and purified by Ni-NTA affinity chromatography. Briefly, cells were resuspended in lysis buffer (20 mM Tris, 500 mM NaCl, 5 mM imidazole, pH 8.0) and 0.5 mM PMSF was added. Cells were lysed using sonication (Misonix XL-2000) and centrifuged at 20,000g for one hour to remove any cellular debris. Supernatant was incubated with Ni-NTA beads for two hours at 4 °C prior to purification and loaded into the column. Impurities were removed by increasing the imidazole concentration in buffer (20 mM Tris pH 8.0, 500 mM NaCl and 6 M urea), 15 mM and 30 mM. Finally, protein was eluted using elution buffer containing 150 mM imidazole followed by buffer exchanged with storage buffer containing 20 mM Tris pH 8.0, 500 mM NaCl, 2 M urea and stored at –80 °C. Concentrated aliquots of protein in storage buffer at –80 °C was thawed on ice and desalted in 20 mM MES buffer pH 6.0 using Zeba Desalting Spin Columns (Thermo) and immediately used for the experiments.

Both unlabeled and ¹⁵N labeled recombinant full-length α S was expressed and purified in Rosetta™ 2 (DE3) pLysS (EMD Millipore®) cells using IMPACT™ system protocol (New England Biolabs®) as described before,⁶⁵ with few modifications. Briefly, α S detached from chitin beads using dithiothreitol (DTT) was eluted in elution buffer (20 mM Tris, 100 mM NaCl, 1 mM EDTA at pH 8.0). The eluted fraction was filtered using 30 kDa centrifugal filter units (Thermo) at 7000g for 20 min. The flow-through was dialyzed against 4L of nanopure water in a 10 kDa dialysis bag to remove DTT and concentrated using a vacufuge. Concentrated α S was directly subjected to reverse phase

HPLC purification by the gradient elution of water and acetonitrile (ACN) each containing 0.1% TFA. HPLC fractions containing pure protein were lyophilized and stored at -80°C . Lyophilized samples were resuspended in 20 mM MES pH 6.0 and subjected to size exclusion chromatography (SEC) to remove any preformed aggregates and thus obtained pure monomeric protein was used as such for studies. Due to better yields, another αS construct containing N-terminus 6-histidine tag and a thrombin cleavage site was also used occasionally in this study. The protein was expressed in BL21 (DE3) cells, purified using Ni-NTA affinity chromatography and concentrated using 10 kDa centrifugal filter unit. Concentrated protein was further subjected to SEC and the fractions corresponding to the monomeric protein were used in the experiments. Unused monomer fractions were stored at 4°C and were used within a week from purification. We confirmed that αS purified using both constructs have similar biophysical characteristics and aggregation kinetics.

Preparation of αS oligomers, αS fibrils and TDP-43 PrLD fibrils

αS oligomers and fibrils were generated similar to previous protocols.^{66,67} Briefly, αS oligomers have been generated by incubating $50\ \mu\text{M}$ αS monomer with 20-fold molar excess of 3,4-Dihydroxyphenylacetaldehyde (DOPAL) at 600 rpm at 37°C for 24 h. Oligomers of αS were isolated using superdex-200 size exclusion chromatography (SEC) column in 10 mM Tris pH 8.0. Fibrils of αS were prepared by incubating 5 mg of monomeric protein in presence of 150 mM NaCl at 600 rpm at 37°C for 7 days. Similarly, TDP-43 PrLD fibrils were generated by incubating $50\ \mu\text{M}$ monomeric TDP-43 in quiescent condition at 37°C for 7 days. Both fibrils were isolated by centrifuging at $20,000g$ for 20 min and stored at -80°C until use.

Thioflavin-T (ThT) fluorescence

Aggregation kinetics were monitored using BioTek Synergy H1 microplate reader. Samples containing $10\ \mu\text{M}$ ThT were excited at 452 nm and emission was monitored at 485 nm at 37°C . The data points were plotted as ThT fluorescence *versus* time and fitted with following Boltzmann sigmoidal function using Origin 8.5.

$$y = A_2 + \frac{(A_1 - A_2)}{1 + e^{(x-x_0)/dx}}$$

In this equation, y corresponds to ThT fluorescence intensity, x is time and x_0 is the time to reach half-maximal ThT fluorescence and A_1 and A_2 are constants. The lag time of aggregation was calculated as $x_0 - 2dx$ for each fitted curve.

SDS-PAGE and immunoblotting

Aliquots of the reactions were subjected to SDS-PAGE and immunoblotting using a monoclonal anti- αS antibody, clone Syn211 (Millipore Sigma). Aliquots of the samples were separately mixed in the 4x Laemmli sample buffer and loaded onto SDS-PAGE Biorad Mini-PROTEAN[®] 4–20% precast gel. Gels were then transferred on to a $0.45\ \mu\text{M}$ Amersham Protran Premium nitrocellulose membrane (GE Life Sciences) and the blot was boiled in 1X PBS for one minute. For dot blot analysis, pellet obtained from αS and TDP-43 co-incubation reaction was treated with formic acid, resuspended in 20 mM MES buffer pH 6.0 and was directly spotted in the nitrocellulose membrane. Blot was then incubated overnight in the blocking buffer (5% non-fat milk, 0.1% Tween[®]-20 in 1X PBS), followed by primary antibodies against αS or TDP-43 PrLD and horseradish peroxidase-conjugated anti-mouse/anti-rabbit secondary antibodies. Finally, images were obtained by treating with ECL reagent using GelDoc molecular imager (Bio-Rad).

MALDI-ToF mass spectrometry

Quantification of αS and TDP-43 PrLD fibrils was performed on a Bruker Datonics Microflex LT/SH MALDI-ToF system. Aliquots of samples from aggregation reactions after 48 h were centrifuged at $18,000g$ for 20 min. The supernatant was discarded and the pellet was washed and resuspended in an equal volume of 20 mM MES buffer pH 6.0. Resuspended pellets were then mixed with an equal volume of formic acid to disaggregate the fibrils. The samples were then mixed with Cytochrome C external standard at $1.42\ \mu\text{M}$ final concentration in 1:1 sinnapinic acid matrix and loaded on to an MSP 96 BC MALDI plate (Bruker Datonics). The instrument was calibrated using Bruker Protein Calibration Standard I (Bruker Datonics) and spectra were collected by adjusting the laser intensity at 70%.

Circular dichroism

Circular dichroism (CD) spectra of $4.25\ \mu\text{M}$ DOPAL-derived αS oligomers in $10\ \mu\text{M}$ Tris buffer pH 8.0 was measured in far UV region (190 to 260 nm) in Jasco J-815 spectrophotometer (Jasco MD) as previously.⁶⁸

Fourier transform infrared (FTIR) spectroscopy

Lyophilized sample of monomeric αS and TDP-43 PrLD along with aggregates from cross-seeding reaction were dissolved in D₂O and subjected to Cary 630 FTIR spectrometer. A total of 1024 scans were collected from $1800\ \text{cm}^{-1}$ to $1400\ \text{cm}^{-1}$ at a resolution of $4\ \text{cm}^{-1}$. Spectra were blank subtracted with D₂O, normalized and plotted in OriginLab 8.0 program.

Dynamic light scattering (DLS)

DLS was carried out in a Zetasizer Nano S instrument (Malvern, Inc.) by averaging 3 runs each of 10 s with a pre-equilibration time of 30 s. Sample volume was kept at 70 μ L in a 1 cm cuvette pathlength. Finally, diameter was determined using volume (%) function and plotted in origin 8.0.

Fluorescence microscopy

Fluorescence microscopic images of the reaction with labeled proteins were obtained using Leica SP8 confocal microscope at 40x magnification in a clear glass bottom 96 well black plates (P96-1.5H-N, Cellvis Inc.). Briefly, protein labeling was carried out by incubating three molar excess of fluorescent dyes, Hilyte 405 or Hilyte 647 (AnaSpec Inc) with the proteins for 12 h at 4 °C. Excess dye was removed using PD SpinTrap™ G-25 (Cytiva Life sciences) columns and the labeled and unlabeled protein samples were mixed in 1:99 ratio and used for the experiments. We do not expect the Hilyte dyes to have any discernable effects on our observations as they are comparable to routinely used xanthane dyes. Moreover, to minimize their effects if any, we used only 1% of total protein with labeled ones in our assays. For thioflavin-S (ThS) staining, aliquots of samples from the reactions were centrifuged at 18,000g for 20 min, and pellets were resuspended in 20 mM MES buffer pH 6.0. ThS was added at a final concentration of 10 μ M and incubated for 10 min prior to imaging.

Fluorescence recovery after photobleaching (FRAP)

Hilyte 647 labeled TDP-43 PrLD and RNA reaction with or without Hilyte 405 labeled α S was monitored using FRAP. The samples were photobleached using 100% laser intensity for 10 seconds with 141 iterations and recovery was monitored for 45 seconds. The FRAP kinetic data was plotted as normalized fluorescence with reference to TDP-43 PrLD and RNA control and was fit using Boltzmann function on Origin 8.5.

NMR spectroscopy

The NMR experiments were carried out using ¹⁵N labeled α S and TDP-43 PrLD in 20 mM MES, pH 6.0 with 10% D₂O after incubation with and without unlabeled TDP-43 PrLD and α S proteins. For these experiments, N-terminus histidine-tag was removed from TDP-43 PrLD using TEV protease.⁵⁵ SOFAST heteronuclear multiple quantum coherence (HMQC)⁶⁹ spectra were obtained on the samples at 10 and 37 °C. The data were acquired on a Bruker Advance- III-HD 850 MHz NMR spectrometer equipped with a Bruker TCI cryoprobe at the high-field NMR facility of the

University of Alabama, Birmingham as described previously.^{70,71} Briefly, SOFAST HMQC was collected as it allows reduction of the recycle delays to 100 ms while maintaining high sensitivity, and decreasing the overall acquisition time.⁶⁹ The protein concentrations were kept at 10 μ M for both proteins with 1:1 molar equivalents of unlabeled proteins added for interaction studies. The spectra were then collected with 2048 data points in F2 (¹H) with 128 scans coadded for each of the 160 F1 (¹⁵N) increments. A ¹J(NH) of 90 Hz was used with a 100 ms relaxation delay. The delay interval from F1 to F2 was set at 0.32 ms. The raw HMQC spectra were processed using Bruker TopSpin 3.5 analysis software with standard methods with phase corrections in both dimensions. Cross-peaks of both α S and TDP-43 PrLD were identified as in previous studies.^{47,55,72}

Atomic force microscopy

AFM images were obtained following a previously published method.⁷³ Briefly, mica was cleaved using tape then attached to a magnet. The mica was then treated with 150 μ L of 3-aminopropyltriethoxysilane (APTES) solution (500 μ L of 3-aminopropyltriethoxysilane in 50 mL of 1 mM acetic acid) for 30 min. The APTES solution was then decanted off and the mica substrate was rinsed three times with nanopure H₂O, dried with N₂, and stored for an hour. The 1–4 μ M reaction samples were diluted to 100-folds and a volume of 150 μ L of the sample solution was deposited onto the mica surface and were allowed to absorb for 30 min. The sample solution was then decanted from the mica surface and washed with 150 μ L of nanopure H₂O three times, dried with N₂, and stored in a desiccator until imaging. AFM analysis was performed using a Dimension Icon atomic force microscope (Bruker) in PeakForce Tapping mode. AFM scanning was performed using NanoScope 8.15r3sr5 software and the images were analyzed in NanoScope Analysis 1.50 software. Imaging was performed using a sharp silicon nitride cantilever (SNL-C, nominal tip radius of 2 nm; nominal resonance frequency of 56 kHz; nominal spring constant of 0.24 N/m) and a standard probe holder under ambient conditions with 512 \times 512 data point resolution. Multiple areas of the mica surface were analyzed, height and phase images were obtained simultaneously, and representative images are reported.

Cell viability XTT assay

Cell viability was measured using 2,3-bis(2-methoxy-4-nitro-5-sulfophenyl)-5-[(phenylamino)carbonyl]-2H-tetrazolium hydroxide (XTT) assay kit (Biotium) following the previously established protocol with few modifications.⁷⁴ Briefly, human neuroblastoma SH-SY5Y cells (ATCC, Manassas, VA) were maintained in a humidified incubator at

37 °C with 5.5% CO₂ in 1:1 mixture of DMEM and Ham's F12K medium with 10% FBS and 1% penicillin/streptomycin. Approximately, 15,000 cells were plated in a clear bottom 96 well black plates (Thermo Scientific) 24 h prior to sample treatment. All the reaction samples were prepared and purified using autoclaved water and buffer to avoid bacterial contamination. Cell medium from wells was replaced with the reaction samples resuspended in complete growth medium and incubated for 24 h prior to XTT assay.

CRedit authorship contribution statement

Shailendra Dhakal: Investigation, Methodology.
Courtney E. Wyant: Investigation, Methodology.
Hannah E. George: Investigation, Methodology.
Sarah E. Morgan: Investigation, Methodology.
Vijayaraghavan Rangachari: Conceptualization, Supervision.

DECLARATION OF COMPETING INTEREST

The authors declare that they have no known competing financial interests or personal relationships that could have appeared to influence the work reported in this paper.

Acknowledgements

The authors would like to thank the following agencies for financial support: National Institute of Aging (1R56AG062292-01) and the National Science Foundation (NSF CBET 1802793) to VR. The authors also thank the National Center for Research Resources (5P20RR01647-11) and the National Institute of General Medical Sciences (8 P20 GM103476-11) from the National Institutes of Health for funding through INBRE for the use of their core facilities.

Declaration of Competing Interest

The authors declare that they have no known competing financial interests or personal relationships that could have appeared to influence the work reported in this paper.

Appendix A. Supplementary material

Supplementary data to this article can be found online at <https://doi.org/10.1016/j.jmb.2021.166953>.

Received 12 December 2020;
 Accepted 17 March 2021;
 Available online 24 March 2021

Keywords:
 α -synuclein;
 TDP-43;
 fibrillization;
 amyloid;
 liquid–liquid phase separation

References

- Soto, C., Estrada, L.D., (2008). Protein misfolding and neurodegeneration. *Arch. Neurol.*, **65**, 184–189.
- Nakamura, T., Lipton, S.A., (2009). Cell death: protein misfolding and neurodegenerative diseases. *Apoptosis.*, **14**, 455–468.
- Sengupta, U., Guerrero-Muñoz, M.J., Castillo-Carranza, D. L., Lasagna-Reeves, C.A., Gerson, J.E., Paulucci-Holthausen, A.A., Krishnamurthy, S., Farhed, M., et al., (2015). Pathological interface between oligomeric alpha-synuclein and tau in synucleinopathies. *Biol. psychiatry.*, **78**, 672–683.
- Galvin, J.E., Lee, V.M.-Y., Trojanowski, J.Q., (2001). Synucleinopathies: clinical and pathological implications. *Arch. Neurol.*, **58**, 186–190.
- Saha, P., Sen, N., (2019). Tauopathy: a common mechanism for neurodegeneration and brain aging. *Mech. Ageing Dev.*, **178**, 72–79.
- Spires-Jones, T.L., Hyman, B.T., (2014). The intersection of amyloid beta and tau at synapses in Alzheimer's disease. *Neuron.*, **82**, 756–771.
- Zhang, J., Mattison, H.A., Liu, C., Ghingina, C., Auinger, P., McDermott, M.P., Stewart, T., Kang, U.J., et al., (2013). Longitudinal assessment of tau and amyloid beta in cerebrospinal fluid of Parkinson disease. *Acta Neuropathol.*, **126**, 671–682.
- Irwin, D.J., Lee, V.M.-Y., Trojanowski, J.Q., (2013). Parkinson's disease dementia: convergence of α -synuclein, tau and amyloid- β pathologies. *Nature Rev. Neurosci.*, **14**, 626–636.
- Vital, A., Canron, M.H., Gil, R., Hauw, J.J., Vital, C., (2007). A sporadic case of Creutzfeldt-Jakob disease with beta-amyloid deposits and alpha-synuclein inclusions. *Neuropathology.*, **27**, 273–277.
- Kovacs, G.G., Rahimi, J., Ströbel, T., Lutz, M.I., Regelsberger, G., Streichenberger, N., Perret-Liaudet, A., Höftberger, R., et al., (2017). Tau pathology in Creutzfeldt-Jakob disease revisited. *Brain pathol.*, **27**, 332–344.
- Hamilton, R.L., (2000). Lewy bodies in Alzheimer's disease: a neuropathological review of 145 cases using α -synuclein immunohistochemistry. *Brain Pathol.*, **10**, 378–384.
- Burré, J., (2015). The synaptic function of α -synuclein. *J. Parkinsons Dis.*, **5**, 699–713.
- Kim, W.S., Kågedal, K., Halliday, G.M., (2014). Alpha-synuclein biology in Lewy body diseases. *Alzheimer's Res. Ther.*, **6**, 73.
- Geser, F., Lee, V.M.-Y., Trojanowski, J.Q., (2010). Amyotrophic lateral sclerosis and frontotemporal lobar degeneration: a spectrum of TDP-43 proteinopathies. *Neuropathology.*, **30**, 103–112.
- Nakashima-Yasuda, H., Uryu, K., Robinson, J., Xie, S.X., Hurtig, H., Duda, J.E., Arnold, S.E., Siderowf, A., et al.,

- (2007). Co-morbidity of TDP-43 proteinopathy in Lewy body related diseases. *Acta Neuropathol.*, **114**, 221–229.
16. Crews, L., Tsigelny, I., Hashimoto, M., Masliah, E., (2009). Role of synucleins in Alzheimer's disease. *Neurotox. Res.*, **16**, 306–317.
 17. Aoki, S., Liu, A.W., Zucca, A., Zucca, S., Wickens, J.R., (2015). Role of striatal cholinergic interneurons in set-shifting in the rat. *J. Neurosci.*, **35**, 9424–9431.
 18. Moussaud, S., Jones, D.R., Moussaud-Lamodière, E.L., Delenclos, M., Ross, O.A., McLean, P.J., (2014). Alpha-synuclein and tau: teammates in neurodegeneration?. *Mol. Neurodegener.*, **9**, 43.
 19. Nonaka, T., Masuda-Suzukake, M., Hasegawa, M., (2018). Molecular mechanisms of the co-deposition of multiple pathological proteins in neurodegenerative diseases. *Neuropathology.*, **38**, 64–71.
 20. Morales, R., Estrada, L.D., Diaz-Espinoza, R., Morales-Scheihing, D., Jara, M.C., Castilla, J., Soto, C., (2010). Molecular cross talk between misfolded proteins in animal models of Alzheimer's and prion diseases. *J. Neurosci.*, **30**, 4528–4535.
 21. Higashi, S., Iseki, E., Yamamoto, R., Minegishi, M., Hino, H., Fujisawa, K., Togo, T., Katsuse, O., et al., (2007). Concurrence of TDP-43, tau and α -synuclein pathology in brains of Alzheimer's disease and dementia with Lewy bodies. *Brain Res.*, **1184**, 284–294.
 22. Schaser, A.J., Osterberg, V.R., Dent, S.E., Stackhouse, T. L., Wakeham, C.M., Boutros, S.W., Weston, L.J., Owen, N., et al., (2019). Alpha-synuclein is a DNA binding protein that modulates DNA repair with implications for Lewy body disorders. *Sci. Rep.*, **9**, 1–19.
 23. Wilson, R.S., Yu, L., Trojanowski, J.Q., Chen, E.-Y., Boyle, P.A., Bennett, D.A., Schneider, J.A., (2013). TDP-43 pathology, cognitive decline, and dementia in old age. *JAMA Neurol.*, **70**, 1418–1424.
 24. Hu, W.T., Josephs, K.A., Knopman, D.S., Boeve, B.F., Dickson, D.W., Petersen, R.C., Parisi, J.E., (2008). Temporal lobar predominance of TDP-43 neuronal cytoplasmic inclusions in Alzheimer disease. *Acta Neuropathol.*, **116**, 215.
 25. Emamzadeh, F.N., (2016). Alpha-synuclein structure, functions, and interactions. *J. Res. Med. Sci.*, **21**
 26. Tian, T., Huang, C., Tong, J., Yang, M., Zhou, H., Xia, X.-G., (2011). TDP-43 potentiates alpha-synuclein toxicity to dopaminergic neurons in transgenic mice. *Int. J. Biol. Sci.*, **7**, 234.
 27. Shen, L., Wang, C., Chen, L., Leung, K.L., Lo, E., Lakso, M., Wong, G., (2020). TDP-1/TDP-43 potentiates human α -Synuclein (HASN) neurodegeneration in *Caenorhabditis elegans*. *Biochim. Biophys. Acta Mol. Basis Dis.*, **165876**
 28. Gallardo, J., Escalona-Noguero, C., Sot, B., (2020). Role of α -synuclein regions in nucleation and elongation of amyloid fiber assembly. *ACS Chem. Neurosci.*, **11**, 872–879.
 29. Stefanis, L., (2012). α -Synuclein in Parkinson's disease. *Cold Spring Harb. Perspect. Med.*, **2**, a009399
 30. François-Moutal, L., Perez-Miller, S., Scott, D.D., Miranda, V.G., Mollasalehi, N., Khanna, M., (2019). Structural Insights Into TDP-43 and Effects of Post-translational Modifications. *Front. Mol. Neurosci.*, **12**
 31. Wang, G., Yang, H., Yan, S., Wang, C.-E., Liu, X., Zhao, B., Ouyang, Z., Yin, P., et al., (2015). Cytoplasmic mislocalization of RNA splicing factors and aberrant neuronal gene splicing in TDP-43 transgenic pig brain. *Mol. Neurodegener.*, **10**, 42.
 32. Buratti, E., Baralle, F.E., (2008). Multiple roles of TDP-43 in gene expression, splicing regulation, and human disease. *Front. Biosci.*, **13**, 8.
 33. Zhang, Y.-J., Xu, Y.-F., Cook, C., Gendron, T.F., Roettges, P., Link, C.D., Lin, W.-L., Tong, J., et al., (2009). Aberrant cleavage of TDP-43 enhances aggregation and cellular toxicity. *Proc. Natl. Acad. Sci.*, **106**, 7607–7612.
 34. Furukawa, Y., Kaneko, K., Nukina, N., (2011). Molecular properties of TAR DNA binding protein-43 fragments are dependent upon its cleavage site. *Biochim. Biophys. Acta Mol. Basis Dis.*, **1812**, 1577–1583.
 35. Neumann, M., Kwong, L.K., Lee, E.B., Kremmer, E., Flatley, A., Xu, Y., Forman, M.S., Troost, D., et al., (2009). Phosphorylation of S409/410 of TDP-43 is a consistent feature in all sporadic and familial forms of TDP-43 proteinopathies. *Acta Neuropathol.*, **117**, 137–149.
 36. Nonaka, T., Kametani, F., Arai, T., Akiyama, H., Hasegawa, M., (2009). Truncation and pathogenic mutations facilitate the formation of intracellular aggregates of TDP-43. *Hum. Mol. Genet.*, **18**, 3353–3364.
 37. Berning, B.A., Walker, A.K., (2019). The pathobiology of TDP-43 C-terminal fragments in ALS and FTL. *Front. Neurosci.*, **13**, 335.
 38. Feneberg, E., Charles, P., Finelli, M., Scott, C., Kessler, B., Fischer, R., Ansorge, O., Gray, E., et al., (2020). Detection and quantification of novel C-terminal TDP-43 fragments in ALS-TDP. *Brain Pathol.*,
 39. Colombrita, C., Zennaro, E., Fallini, C., Weber, M., Sommacal, A., Buratti, E., Silani, V., Ratti, A., (2009). TDP-43 is recruited to stress granules in conditions of oxidative insult. *J. Neurochem.*, **111**, 1051–1061.
 40. Bhopatkar, A.A., Uversky, V.N., Rangachari, V., (2020). Granulins modulate liquid-liquid phase separation and aggregation of prion-like C-terminal domain of the neurodegeneration-associated protein TDP-43. *J. Biol. Chem. jbc.*, **RA119**, 011501
 41. Mompean, M., Chakrabarty, A., Buratti, E., Laurents, D.V., (2016). Electrostatic repulsion governs TDP-43 C-terminal domain aggregation. *PLoS Biol.*, **14**
 42. Berning, B.A., Walker, A.K., (2019). The pathobiology of TDP-43 C-terminal fragments in ALS and FTL. *Front. Neurosci.*, **13**
 43. Miklos, A.C., Sumpter, M., Zhou, H.-X., (2013). Competitive interactions of ligands and macromolecular crowders with maltose binding protein. *PLoS One*, **8**, e74969
 44. Diniz, A., Dias, J.S., Jiménez-Barbero, J., Marcelo, F., Cabrita, E.J., (2017). Protein–glycan quinary interactions in crowding environment unveiled by NMR spectroscopy. *Chem. Eur. J.*, **23**, 13213–13220.
 45. Ghosh, P., Kumar, A., Datta, B., Rangachari, V., (2010). Dynamics of protofibril elongation and association involved in A β 42 peptide aggregation in Alzheimer's disease. *BMC Bioinform.*, **11**, S24.
 46. Walker, A.K., Soo, K.Y., Sundaramoorthy, V., Parakh, S., Ma, Y., Farg, M.A., Wallace, R.H., Crouch, P.J., et al., (2013). ALS-associated TDP-43 induces endoplasmic reticulum stress, which drives cytoplasmic TDP-43 accumulation and stress granule formation. *PLoS one*, **8**, e81170
 47. Dasari, A.K., Kaye, R., Wi, S., Lim, K.H., (2019). Tau interacts with the C-terminal region of α -synuclein, promoting formation of toxic aggregates with distinct molecular conformations. *Biochemistry*, **58**, 2814–2821.

48. Igaz, L.M., Kwong, L.K., Xu, Y., Truax, A.C., Uryu, K., Neumann, M., Clark, C.M., Elman, L.B., et al., (2008). Enrichment of C-terminal fragments in TAR DNA-binding protein-43 cytoplasmic inclusions in brain but not in spinal cord of frontotemporal lobar degeneration and amyotrophic lateral sclerosis. *Am. J. Pathol.*, **173**, 182–194.
49. Porta, S., Xu, Y., Restrepo, C.R., Kwong, L.K., Zhang, B., Brown, H.J., Lee, E.B., Trojanowski, J.Q., et al., (2018). Patient-derived frontotemporal lobar degeneration brain extracts induce formation and spreading of TDP-43 pathology in vivo. *Nature Commun.*, **9**, 1–15.
50. Feneberg, E., Gray, E., Ansoorge, O., Talbot, K., Turner, M. R., (2018). Towards a TDP-43-based biomarker for ALS and FTLD. *Mol. Neurobiol.*, **55**, 7789–7801.
51. Tsuji, H., Nonaka, T., Yamashita, M., Masuda-Suzukake, M., Kametani, F., Akiyama, H., Mann, D.M., Tamaoka, A., et al., (2012). Epitope mapping of antibodies against TDP-43 and detection of protease-resistant fragments of pathological TDP-43 in amyotrophic lateral sclerosis and frontotemporal lobar degeneration. *Biochem. Biophys. Res. Commun.*, **417**, 116–121.
52. Yang, C., Tan, W., Whittle, C., Qiu, L., Cao, L., Akbarian, S., Xu, Z., (2010). The C-terminal TDP-43 fragments have a high aggregation propensity and harm neurons by a dominant-negative mechanism. *PLoS one*, **5**, e15878
53. Xiao, S., Sanelli, T., Chiang, H., Sun, Y., Chakrabarty, A., Keith, J., Rogava, E., Zinman, L., et al., (2015). Low molecular weight species of TDP-43 generated by abnormal splicing form inclusions in amyotrophic lateral sclerosis and result in motor neuron death. *Acta Neuropathol.*, **130**, 49–61.
54. McDonald, K.K., Aulas, A., Destroismaisons, L., Pickles, S., Belec, E., Camu, W., Rouleau, G.A., Vande Velde, C., (2011). TAR DNA-binding protein 43 (TDP-43) regulates stress granule dynamics via differential regulation of G3BP and TIA-1. *Hum. Mol. Genet.*, **20**, 1400–1410.
55. Conicella, A.E., Zerze, G.H., Mittal, J., Fawzi, N.L., (2016). ALS mutations disrupt phase separation mediated by α -helical structure in the TDP-43 low-complexity C-terminal domain. *Structure*, **24**, 1537–1549.
56. Molliex, A., Temirov, J., Lee, J., Coughlin, M., Kanagaraj, A.P., Kim, H.J., Mittag, T., Taylor, J.P., (2015). Phase separation by low complexity domains promotes stress granule assembly and drives pathological fibrillization. *Cell.*, **163**, 123–133.
57. Meyerowitz, J., Parker, S.J., Vella, L.J., Ng, D.C., Price, K. A., Liddell, J.R., Caragounis, A., Li, Q.-X., et al., (2011). C-Jun N-terminal kinase controls TDP-43 accumulation in stress granules induced by oxidative stress. *Mol. Neurodegener.*, **6**, 57.
58. Cappai, R., Leck, S.L., Tew, D.J., Williamson, N.A., Smith, D.P., Galatis, D., Sharpies, R.A., Curtain, C.C., et al., (2005). Dopamine promotes α -synuclein aggregation into SDS-resistant soluble oligomers via a distinct folding pathway. *FASEB J.*, **19**, 1377–1379.
59. Sengupta, U., Puangmalai, N., Bhatt, N., Garcia, S., Zhao, Y., Kayed, R., (2020). Polymorphic α -synuclein strains modified by dopamine and docosahexaenoic acid interact differentially with tau protein. *Mol. Neurobiol.*, **57**, 2741–2765.
60. Rekas, A., Knott, R.B., Sokolova, A., Barnham, K.J., Perez, K.A., Masters, C.L., Drew, S.C., Cappai, R., et al., (2010). The structure of dopamine induced α -synuclein oligomers. *Eur. Biophys. J.*, **39**, 1407–1419.
61. Gao, J., Wang, L., Huntley, M.L., Perry, G., Wang, X., (2018). Pathomechanisms of TDP-43 in neurodegeneration. *J. Neurochem.*, **146**, 7–20.
62. Jo, M., Lee, S., Jeon, Y.-M., Kim, S., Kwon, Y., Kim, H.-J., (2020). The role of TDP-43 propagation in neurodegenerative diseases: integrating insights from clinical and experimental studies. *Exp. Mol. Med.*, **52**, 1652–1662.
63. Visanji, N.P., Lang, A.E., Kovacs, G.G., (2019). Beyond the synucleinopathies: alpha synuclein as a driving force in neurodegenerative comorbidities. *Transl. Neurodegener.*, **8**, 28.
64. Koga, S., Lin, W.L., Walton, R.L., Ross, O.A., Dickson, D. W., (2018). TDP-43 pathology in multiple system atrophy: colocalization of TDP-43 and α -synuclein in glial cytoplasmic inclusions. *Neuropathol. Appl. Neurobiol.*, **44**, 707–721.
65. Planchard, M.S., Exley, S.E., Morgan, S.E., Rangachari, V., (2014). Dopamine-induced α -synuclein oligomers show self- and cross-propagation properties. *Protein Sci.*, **23**, 1369–1379.
66. Plotegher, N., Berti, G., Ferrari, E., Tessari, I., Zanetti, M., Lunelli, L., Greggio, E., Bisaglia, M., et al., (2017). DOPAL derived alpha-synuclein oligomers impair synaptic vesicles physiological function. *Sci. Rep.*, **7**, 1–16.
67. Strohäker, T., Jung, B.C., Liou, S.-H., Fernandez, C.O., Riedel, D., Becker, S., Halliday, G.M., Bennati, M., et al., (2019). Structural heterogeneity of α -synuclein fibrils amplified from patient brain extracts. *Nature Commun.*, **10**, 1–12.
68. Dhakal, S., Sapkota, K., Huang, F., Rangachari, V., (2020). Cloning, expression and purification of the low-complexity region of RanBP9 protein. *Protein Express. Purif.*, 105630.
69. Schanda, P., (2005). Kupfçe f, Brutscher B. SOFAST-HMQC experiments for recording two-dimensional heteronuclear correlation spectra of proteins within a few seconds. *J. Biomol. NMR*, **33**, 199–211.
70. Bhopatkar, A.A., Uversky, V.N., Rangachari, V., (2020). Granulins modulate liquid–liquid phase separation and aggregation of the prion-like C-terminal domain of the neurodegeneration-associated protein TDP-43. *J. Biol. Chem.*, **295**, 2506–2519.
71. Ghag, G., Holler, C.J., Taylor, G., Kukar, T.L., Uversky, V. N., Rangachari, V., (2017). Disulfide bonds and disorder in granulin-3: an unusual handshake between structural stability and plasticity. *Protein Sci.*, **26**, 1759–1772.
72. Wu, K.-P., Baum, J., (2011). Backbone assignment and dynamics of human α -synuclein in viscous 2 M glucose solution. *Biomol. NMR Assign.*, **5**, 43–46.
73. Dean, D.N., Das, P.K., Rana, P., Burg, F., Levites, Y., Morgan, S.E., Ghosh, P., Rangachari, V., (2017). Strain-specific fibril propagation by an A β dodecamer. *Sci. Rep.*, **7**, 40787.
74. Saha, J., Dean, D.N., Dhakal, S., Stockmal, K.A., Morgan, S.E., Dillon, K.D., Adamo, M.F., Levites, Y., et al., (2021). Biophysical characteristics of lipid-induced A β oligomers correlate to distinctive phenotypes in transgenic mice. *FASEB J.*, **35**, e21318.